Mon. Not. R. astr. Soc. (1989) **240**, *Short Communication*, 7P–24P

Spectroscopic and photometric observations of SN1987A – VI. Days 617 to 792

P. A. Whitelock,[1] R. M. Catchpole,[1] J. W. Menzies,[1] M. W. Feast,[1] S. E. Woosley,[2] D. A. Allen,[3] F. van Wyk,[1] F. Marang,[1] C. D. Laney,[1] H. Winkler,[4] K. Sekiguchi,[1] L. A. Balona,[1] B. S. Carter,[1] J. H. Spencer Jones,[1] J. D. Laing,[1] T. Lloyd Evans,[1] A. P. Fairall,[4] D. A. H. Buckley,[4] I. S. Glass,[1] M. V. Penston,[5] L. N. da Costa,[6] S. A. Bell,[7] C. Hellier,[8] M. Shara[9] and A. F. J. Moffat[10]

[1] *South African Astronomical Observatory, PO Box 9, Observatory 7935, South Africa*
[2] *Lick Observatory, University of California, Santa Cruz, CA 95064, USA*
[3] *Anglo-Australian Observatory, PO Box 296, Epping, NSW 2121, Australia*
[4] *Astronomy Department, University of Cape Town, Private Bag, Rondebosch 7700, South Africa*
[5] *Royal Greenwich Observatory, Madingley Road, Cambridge CB3 0EZ*
[6] *Observatório Nacional, Rua General Jose Cristino 77, 20921, São Cristovao, Rio de Janeiro, Brazil*
[7] *University Observatory, Buchanan Gardens, St Andrews, Fife KY16 9LZ*
[8] *Mullard Space Science Laboratory, Holmbury St Mary, Dorking, Surrey RH5 6NT*
[9] *Space Telescope Science Institute, 3700 San Martin Drive, Baltimore, MD 21218, USA*
[10] *Département de Physique, Université de Montréal, CP6128 Succ. A, Montréal, PQ H3C 3J7, Canada*

Accepted 1989 June 21. Received 1989 June 13; in original form 1989 May 8

Summary. We present spectroscopic and $UBV(RI)_C JHKLM$ photometric observations of SN1987A in the Large Magellanic Cloud made between days 617 and 792 after the Kamiokande-II neutrino event. During the period from day 520 to day 630 the U to M bolometric flux went through a very steep decline, returning after day 670 to the same decline rate as before day 500. Various explanations for these changes are examined. The addition of the supernova output at high energies (derived from models of X-ray and γ-ray data) to that from the U to M spectral region leaves a deficit from the predicted radioactive decay energy after day 500. This deficit can apparently be accounted for if the far-infrared dust emission is also added to the energy

budget. There is no compelling evidence for the presence of any additional energy source, such as a pulsar, during this period. However, the errors on the total luminosity are sufficiently high that the presence of a source radiating at a level less than 10^{38} erg s^{-1} cannot be excluded.

1 Introduction

Spectroscopic and photometric observations of SN1987A made at the Sutherland Observatory of the SAAO for the first 616 d after its discovery were presented by Menzies *et al.* (1987), Catchpole *et al.* (1987, 1988), Whitelock *et al.* (1988) and Catchpole *et al.* (1989) (hereafter Papers I, II, III, IV and V). In the present paper we give the SAAO data for the period from day 617 to day 792 together with some infrared photometry from the AAO. As in papers II to V we adopt the Kamiokande-II neutrino event as the epoch of the supernova outburst (JD 2446849.816, February 23.316 1987). A distance modulus for the LMC of 18.5 and an interstellar absorption of $A_v = 0.6$ are also used.

2 Spectroscopic data

As previously, spectra have been obtained with a two-channel intensified Reticon detector on the grating spectrograph at the Cassegrain focus of the 1.9-m telescope at Sutherland. A 300 line mm^{-1} grating was used in the first order with a slit width of 300 μm to give a resolution of 7 Å (FWHM). The instrumental flux calibration was obtained from an observation of a spectrophotometric standard each night. The supernova spectra were corrected to a flux scale and multiplied by a suitable factor to give a V magnitude which agreed with the observed or interpolated photometric magnitude for the relevant night. The calendar and Julian dates on which spectra were obtained are listed in Table 1. Some of the spectra are shown in Fig. 1.

Throughout the period discussed here the spectra are characteristic of the 'supernebular' phase of type II supernova. The continuum declined and almost disappeared and the broad Hα line dominates the spectrum. The [O I] $\lambda\lambda$6300, 6364 lines declined more rapidly than either Hα or the [Ca II] λ7291–7324 lines. In the blue [Mg I] λ4571 is prominent, and is superposed on a broad band of emission probably due to blended Fe II lines.

Narrow [O III], $\lambda\lambda$4959, 5007, [N II], $\lambda\lambda$6548, 6584, [Ne III] λ3869, Hα and Hβ emission lines have become prominent as the supernova has faded. These are all unresolved in our spectra and are coming from material essentially at rest with respect to the LMC. The [O III] lines are at least 10 times stronger than those from our two sky comparison regions 30 arcsec east and west of the supernova. The latter emission comes from the gas of the 30 Dor complex which appears in the foreground of the supernova. The narrow supernova lines presumably

Table 1. Heliocentric Julian dates of spectra.

Date	(2440000+)	Date	(2440000+)
1988 Nov 9	7475.61	1989 Feb 1	7559.36
30	7496.44	11	7569.54
Dec 12	7507.47	28	7586.23
30	7525.45	Mar 5	7591.27
1989 Jan 3	7529.45	9	7595.34
8	7534.56	Apr 5	7622.25
14	7540.56		

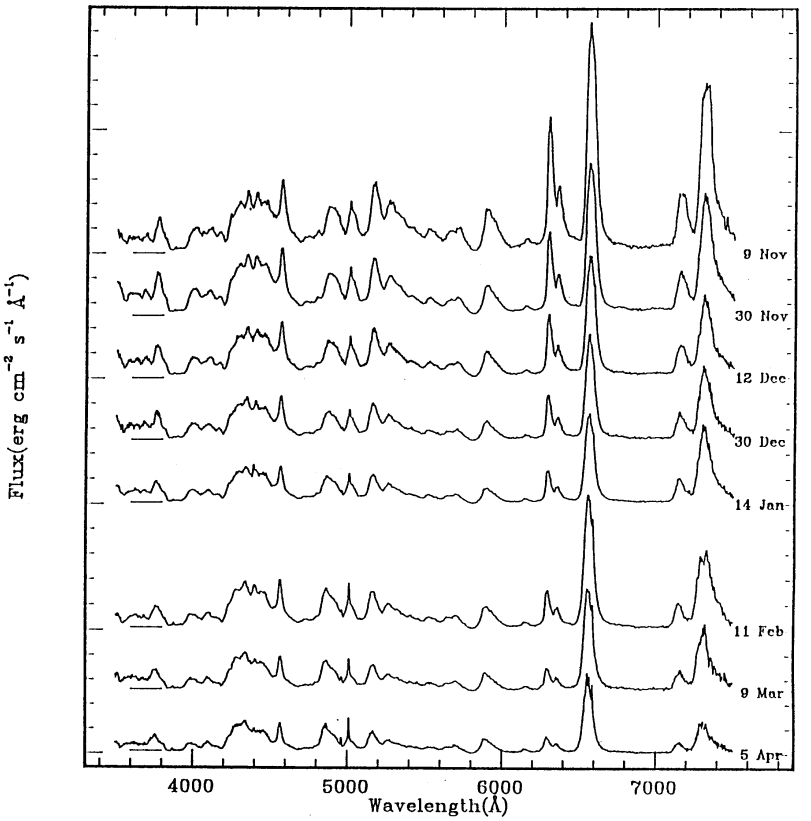

Figure 1. Some of the spectra of SN1987A obtained during the period under discussion. Tick marks on the vertical axis represent a flux of 2.0×10^{-13} erg cm^{-2} s^{-1} A^{-1} for the top five spectra and half of this for the bottom three. Successive spectra have been displaced vertically for clarity of display and the zero for each is shown as a short horizontal bar on the left.

originate in the same region as do those of He II, C III, N III, N IV, N V and O III seen in the short wavelength *IUE* spectra (Kirshner 1987). This region is probably at the interface between the slow moving red-supergiant and the fast blue-supergiant winds emitted by the supernova progenitor at successive phases of its evolution. Its energy source is most likely to be the EUV burst at the time of shock breakout from the surface of the progenitor (Fransson *et al.* 1989).

3 Photometry

3.1 PHOTOELECTRIC PHOTOMETRY

The $UBV(RI)_C$ data are listed in Table 2. As in Papers I–V these were obtained with the single-channel Modular photometer, standard filters and Hamamatsu R943-02 GaAs photomultiplier mounted on the 0.5-m reflector at Sutherland. As in the previous papers, the data were reduced using standard colour equations and the zero points were determined from observations of two nearby standards CPD-68°375 and CPD-61°517.

During the period under consideration the supernova was sufficiently faint for contamination, by optical companions and by stars in the sky aperture, to have become a problem. In an attempt to minimize contamination effects the measurement aperture was reduced from 30 to 25 arcsec from 1988 December 20/21 (JD 2447516). In addition, a different sky comparison region was used for each of two measurements of the supernova. The regions were selected from CCD frames to contain a low background star density and are located about 45 arcsec

Table 2. $UBV(RI)_C$ photometry of SN1987A.

JD 2447000+	V	(B-V)	(U-B)	(V-R)c	(V-I)c	JD 2447000+	V	(B-V)	(U-B)	(V-R)c	(V-I)c
467.428	10.28	0.40	0.01	0.55	0.85	545.298	11.60	0.16	-0.15	0.54	0.95
469.481	10.28	0.38	-0.03	0.53	0.85	548.314	11.65	0.21	-0.17	0.52	0.93
470.473	10.36	0.39	0.03	0.55	0.88	549.298	11.68	0.18	-0.16	0.54	0.95
473.566	10.43	0.37	0.01	0.56	0.88	550.432	11.69	0.17	-0.16	0.55	0.96
475.438	10.44	0.38	-0.01	0.54	0.87	551.318	11.68	0.20	-0.20	0.53	0.93
476.434	10.46	0.37	-0.01	0.56	0.89	552.316	11.70	0.18	-0.20	0.55	0.95
477.436	10.48	0.37	-0.03	0.54	0.87	553.314	11.70	0.17	-0.20	0.53	0.95
478.484	10.50	0.37	-0.01	0.55	0.88	554.320	11.72	0.17	-0.21	0.54	0.94
480.464	10.53	0.35	-0.04	0.55	0.87	555.338	11.75	0.16	-0.17	0.54	0.94
481.522	10.51	0.35	-0.10	0.52	0.83	559.334	11.78	0.17	-0.18	0.53	0.94
483.517	10.56	0.34	-0.07	0.53	0.86	560.298	11.80	0.17	-0.19	0.52	0.93
484.565	10.59	0.34	-0.07	0.53	0.86	561.295	11.82	0.18	-0.18	0.54	0.96
485.569	10.60	0.35	-0.08	0.53	0.85	562.322	11.85	0.17	-0.17	0.53	0.95
486.479	10.61	0.34	-0.09	0.53	0.85	563.370	11.85	0.16	-0.19	0.52	0.94
487.423	10.62	0.31	-0.09	0.52	0.83	564.294	11.87	0.16	-0.20	0.53	0.94
492.421	10.76	0.31	-0.04	0.53	0.88	566.379	11.85	0.16	-0.24	0.53	0.91
494.413	10.79	0.32	-0.07	0.53	0.89	567.345	11.89	0.17	-0.22	0.52	0.94
495.405	10.81	0.31	-0.08	0.54	0.90	570.302	11.92	0.14	-0.22	0.53	0.93
496.462	10.80	0.30	-0.10	0.52	0.87	579.293	12.06	0.13	-0.22	0.54	0.95
497.546	10.81	0.30	-0.11	0.53	0.88	580.297	12.07	0.15	-0.23	0.52	0.92
498.426	10.85	0.30	-0.08	0.52	0.87	581.298	12.09	0.15	-0.23	0.54	0.95
499.326	10.87	0.28	-0.08	0.53	0.87	583.299	12.11	0.14	-0.23	0.51	0.92
501.474	10.87	0.29	-0.12	0.51	0.86	584.294	12.13	0.11	-0.22	0.54	0.94
502.384	10.90	0.30	-0.10	0.52	0.89	586.338	12.13	0.12	-0.24	0.51	0.92
506.540	10.94	0.30	-0.15	0.52	0.88	588.295	12.17	0.13	-0.23	0.52	0.95
507.542	10.99	0.27	-0.15	0.52	0.88	590.316	12.18	0.10	-0.26	0.53	0.93
509.341	11.03	0.26	-0.12	0.53	0.88	591.288	12.19	0.12	-0.24	0.53	0.93
510.520	11.03	0.28	-0.13	0.50	0.87	592.299	12.23	0.10	-0.25	0.53	0.94
512.327	11.07	0.27	-0.12	0.52	0.89	593.285	12.21	0.12	-0.28	0.52	0.91
513.450	11.08	0.25	-0.12	0.52	0.89	594.306	12.24	0.10	-0.22	0.52	0.92
516.386	11.14	0.27	-0.13	0.52	0.89	596.271	12.25	0.10	-0.26	0.54	0.93
517.368	11.16	0.26	-0.13	0.54	0.89	597.313	12.26	0.11	-0.24	0.51	0.93
518.366	11.18	0.27	-0.13	0.52	0.85	601.274	12.24	0.12	-0.31	0.49	0.86
521.358	11.22	0.27	-0.15	0.52	0.91	602.279	12.24	0.11	-0.28	0.48	0.86
524.362	11.26	0.26	-0.15	0.52	0.89	607.274	12.36	0.10	-0.26	0.53	0.89
525.360	11.27	0.25	-0.16	0.52	0.88	608.273	12.39	0.13	-0.24	0.52	0.92
526.362	11.30	0.25	-0.16	0.52	0.90	609.267	12.41	0.13	-0.25	0.54	0.90
530.390	11.38	0.23	-0.14	0.53	0.91	617.262	12.47	0.11	-0.29	0.51	0.88
532.445	11.41	0.21	-0.13	0.53	0.93	618.260	12.48	0.12	-0.29	0.51	0.87
533.416	11.43	0.22	-0.15	0.53	0.94	619.258	12.52	0.08	-0.24	0.51	0.86
534.417	11.44	0.22	-0.17	0.53	0.94	620.260	12.52	0.11	-0.27	0.53	0.89
535.405	11.46	0.21	-0.15	0.52	0.93	621.268	12.58	0.07	-0.29	0.57	0.92
536.325	11.47	0.22	-0.15	0.53	0.91	622.245	12.57	0.10	-0.30	0.53	0.88
537.370	11.49	0.22	-0.14	0.54	0.94	629.262	12.62	0.08	-0.33	0.53	0.82
538.336	11.48	0.21	-0.17	0.52	0.92	634.226	12.67	0.06	-0.31	0.52	0.85
539.296	11.48	0.17	-0.13	0.51	0.92	641.225	12.71	0.08	-0.31	0.52	0.81
540.380	11.51	0.21	-0.18	0.52	0.92						
541.315	11.52	0.21	-0.17	0.52	0.92						
542.380	11.54	0.20	-0.18	0.53	0.92						
543.300	11.54	0.19	-0.16	0.52	0.92						

north and 100 arcsec east of the supernova. From 1989 March 21/22 (JD 2447607) a 20 arcsec aperture was used. From scatter in the differences of the two measurements the rms error is between 0.02 and 0.03 mag and there are possible systematic effects of the order of 0.01 mag due to the differences in the sky regions.

3.2 INFRARED PHOTOMETRY

The infrared photometry obtained with the SAAO 1.9-m telescope is listed in Table 3. HR 1953 was used as a comparison star (see Paper V). The internal observational errors are less than ± 0.02 mag in J, H and K and ± 0.06 in L, L' and M, unless the magnitude is given in parentheses in which case the error is less than ± 0.1 mag. A small number of infrared

Table 3. Infrared photometry of SN1987A with 1.9 m.

JD 2447000+	J	H	K	L	L′	M
473.57	9.14	8.65	9.28	7.44	6.78	4.52
483.30	9.29	8.82	9.41	7.56	6.90	4.66
484.30	9.32	8.83	9.44	7.61	6.95	4.69
486.50	9.36	8.88	9.50	7.67	7.02	4.75
487.31				7.73	7.01	4.69
495.30	9.51	9.05	9.68	8.01	7.27	4.81
502.46				8.21	7.48	4.99
509.48	9.73	9.28	9.90	8.36	7.50	5.05
512.38	9.74	9.35	9.94			
513.47	9.73	9.35	9.97			
516.34	9.80	9.40	10.02	8.55	7.73	5.27
517.43	9.83	9.41	10.06	8.63	(7.64)	(5.36)
518.38	9.81	9.42	10.05	8.61	7.91	(5.36)
521.40	9.88	9.47	10.08	8.65	7.95	5.40
536.33	10.01	9.66	10.27	(9.03)	(8.16)	(5.72)
543.32	10.10	9.76	10.35	(8.99)	(8.37)	(5.66)
550.43	10.20	9.88	10.51	(9.38)	(8.63)	(5.87)
566.39	10.33	10.03	10.68	(9.44)		(6.08)
581.26	10.55	10.23	10.88	9.81		(6.51)
593.38	10.66	10.34	11.01	10.04		(6.70)
601.28	10.70	10.41	11.08	(10.16)		(6.72)
607.24	10.78	10.51	11.17	10.15		6.85
608.23	10.77	10.50	11.16	10.16		6.77
609.26	10.83	10.53	11.20	(10.25)		(6.87)
617.22	10.90	10.63	11.28	10.27		7.01
619.22	10.93	10.63	11.29	10.31		7.07
620.22	10.93	10.64	11.30	10.36		7.01
635.22	11.05	10.81	11.43	(10.35)		(7.26)
641.20	11.13	10.87	11.53	(10.41)		(7.41)

Table 4. JHK photometry of SN1987A with 0.75 m.

JD 2447000+	J	H	K
490.52	9.39	8.91	9.50
492.33	9.62	8.97	9.58
494.30	9.56	9.06	9.71
495.32	9.55	9.05	9.71

observations obtained on the SAAO 0.75-m are listed in Table 4. During the acquisition of these data a contaminating source was discovered in one of the two sky apertures of the 0.75-m infrared photometer. The infrared colours of this source were measured on the 1.9-m at $J = 12.48$, $H = 11.75$ and $K = 11.61$. A correction for the effect of this source has been applied to the data in Table 4. A similar correction must be applied to the data in table 3 of Paper V (i.e. a flux represented by the following magnitudes must be added to the supernova fluxes as represented by the tabulated magnitudes: $J = 13.23$; $H = 12.50$; $K = 12.36$). This is a small effect, changing the faintest *JHK* magnitudes in Paper V, those obtained on JD 2447466.39 by only 0.024, 0.028 and 0.059 mag, respectively. The data in Table 4 are accurate to ± 0.04 mag.

Observations obtained at the AAT are given in Table 5. They were reduced with respect to HR 2015 ($J = 3.88$, $H = 3.76$, $K = 3.72$, $L' = 3.69$, $M = 3.68$) and are accurate to ± 0.02 in *J*, *H*,

Table 5. AAO infrared photometry.

2447000+	J	H	K	L'	M
			(mag)		
425.33	8.29	7.88	8.38	6.05	3.88
545.87	10.14	9.92	10.43	8.47	5.86
584.90	10.60	10.37	10.95	9.31	6.42

K, L' and ± 0.04 in M. The differences between the SAAO and AAO photometry are due to the slightly different photometric systems in use at the two observatories and are no more than is to be expected given the energy distribution of the supernova.

4 Bolometric luminosity

Before the bolometric flux was calculated the measured magnitudes were corrected for contamination by the two nearby B stars (# 2 and # 3 of West 1987, 2.9 and 1.5 arcsec from SN1987A). These corrections, given in Table 6, were evaluated on the assumption that the two stars have the following spectral types and V magnitudes (Walborn *et al.* 1987; Gilmozzi 1987): # 2 BOV, $V=15.29$; # 3 B1.5V, $V=15.68$, and that the interstellar extinction is $A_v=0.6$. When the supernova has faded it will be possible to measure the colours of the contaminating stars more accurately. However, it is unlikely that the results reported here will need to be changed significantly as the supernova was much brighter than its companions over the period considered.

Table 7 gives two versions of the bolometric magnitude derived by integrating spline fits to the U to L and to the U to M data sets. The methods of fitting the data, the flux calibration and sources of uncertainty have been discussed in Papers II to V. The luminosity may be calculated from the magnitude using the expression given in Paper V.

It would seem that the method likely to give the most realistic representation of the true bolometric flux during this phase, as well as that covered by Papers IV and V, is the U to M spline fit. However, this conclusion depends on the origin of the flux in the M band, as is discussed below (Section 6).

As explained in Paper III, when spline fits are used to derive the bolometric flux the contribution from the ultraviolet (wavelengths shorter than those covered by the U band) is estimated by extrapolating the trend between the B and U bands. With the exception of the first few days after outburst the ultraviolet flux derived in this way and confirmed by *IUE* observations was a very small fraction of the total energy output. In recent times $U-B$ has

Table 6. Combined magnitudes of the two B stars close to SN1987A.

Band	Mag	Band	Mag
U	13.81	J	14.96
B	14.64	H	14.99
V	14.72	K	15.03
R	14.69	L	15.07
I	14.69		

Table 7. SN1987A bolometric magnitudes from spline fits.

Time Day	U to L	U to M
623.74	9.85	9.56
633.59	9.97	9.68
634.61	9.99	9.71
636.67	10.03	9.74
645.54	10.20	9.89
659.59	10.43	10.11
666.55	10.54	10.26
667.58	10.56	10.29
668.55	10.58	10.31
671.56	10.61	10.34
686.58	10.84	10.59
693.58	10.90	10.62
700.68	11.05	10.78
716.56	11.19	10.94
731.46	11.44	11.22
743.51	11.55	11.35
751.46	11.60	11.39
757.44	11.73	11.52
758.43	11.76	11.53
759.44	11.79	11.57
767.42	11.85	11.65
769.42	11.90	11.70
770.42	11.91	11.69
791.38	12.11	11.94

decreased and the implied ultraviolet contribution to the total flux therefore increased. On day 770, six per cent of the energy originated shortward of the *U* band, as derived from *U* to *M* spline fits. An extrapolation of data obtained with the *IUE* (Kirshner 1989, private communication) suggests that the ultraviolet contribution is actually somewhat larger, about 15 per cent of the *U* to *M* flux on day 770. This, however, is strongly dependent on the assumed reddening and the correction due to contamination by stars # 2 and # 3. It is clear that future estimates of the bolometric magnitude must take the ultraviolet contribution into consideration.

Details of changes in the e-folding time of the bolometric flux are given in Table 8. It is clear from this that the decay rate prior to day 500 and after day 700 was more or less the same while a much steeper drop occurred in the intervening period. The steepest part of the drop was between days 520 and 630.

Table 8. e-folding times for the bolometric light curve.

Period (day)	U to M	U to M*	U to L
300–400	99.1 ± 0.3	99.1 ± 0.3	98.0 ± 0.2
400–500	90.0 ± 0.6	88.9 ± 0.7	88.0 ± 0.3
500–600	65.3 ± 0.5	60.0 ± 0.6	61.1 ± 0.4
600–700	66.2 ± 0.8	68.2 ± 1.0	66.8 ± 0.8
700–792	82.8 ± 2.3	88.3 ± 2.7	88.9 ± 2.8

*Dust emission subtracted from the *M* band.

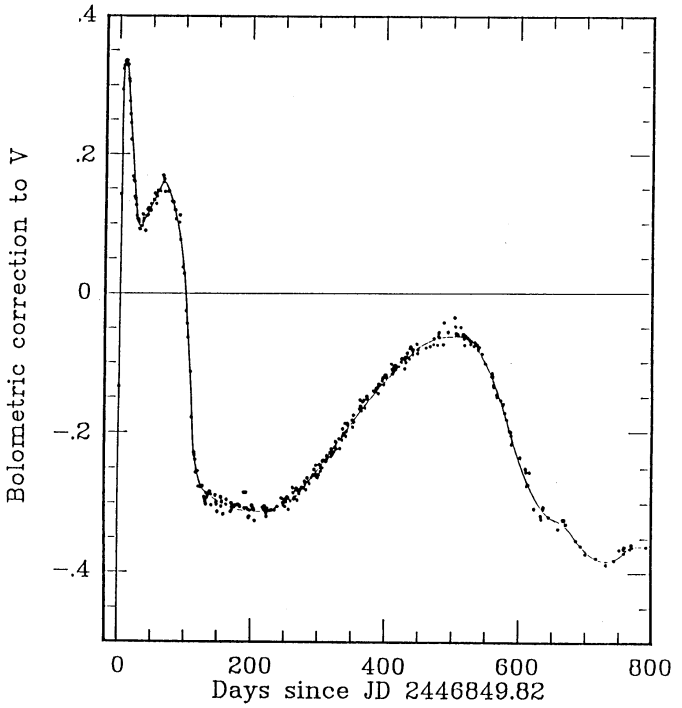

Figure 2. The bolometric correction ($BC = M_{bol} - V_0$) as a function of time.

4.1 BOLOMETRIC CORRECTION

At various times the suggestion has been made of supernovae, and in particular of SN1987A, that the V magnitude provides an adequate representation of the bolometric magnitude. Indeed, in view of the problems involved in multi-wavelength measurement, the task of monitoring the bolometric behaviour of a supernova would be greatly simplified if this were the case. Fig. 2 is a plot of the bolometric correction, $BC = M_{bol} - V_0$, against time. The first few points are overestimated, i.e. they should be more negative, due to the exclusion of the then very strong far-ultraviolet flux from the bolometric magnitude calculations. The accuracy of the most recent points is subject to the uncertainties discussed below. Nevertheless Fig. 2 demonstrates the gross changes in the bolometric correction with time and hence the inadequacy of V as a measure of the U to M bolometric flux.

5 Colour changes

Fig. 3 illustrates the colour changes which took place between days 400 and 792. $B-V$, $(V-R)_C$ and $(V-I)_C$ show very similar trends to $U-B$, though over a smaller range. $J-H$ and $H-K$ show very little variation over the period.

The variation in the optical colours appears to be associated with the bolometric flux changes noted above (Section 4), in the sense that the colours became bluer during the rapid fading. The decrease in $K-L$ appears to coincide with the end of the rapid fading. These colour changes are not accompanied by any gross changes in line excitation in the optical spectra.

6 Far-infrared contribution

It is clear from observations made with the KAO (Witteborn *et al.*, private communication; Moseley *et al.* 1989) and at the AAO (Roche *et al.* 1989; Roche, private communication) that

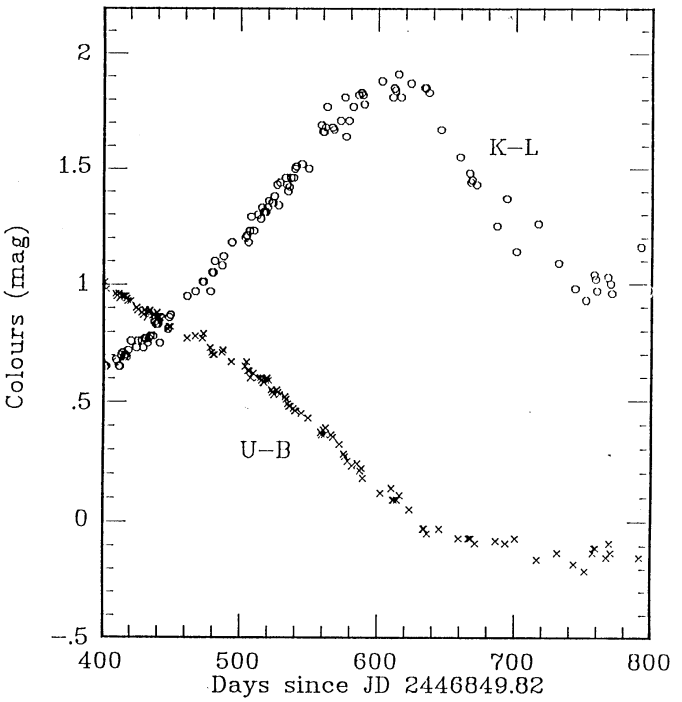

Figure 3. SN1987A colour changes.

after day 450 the supernova was emitting a considerable flux longward of 6 μm, hereafter referred to as the far-infrared. This flux probably arises from heated dust which will almost certainly produce some contribution to the flux in the *M* band. Whether this contribution should be subtracted before calculating the bolometric magnitudes or whether all of the far-infrared should be included in the bolometric integral depends on the location of the dust. The two extreme possibilities are discussed below.

6.1 LIGHT-ECHO

The far-infrared flux may represent a light echo from material behind the supernova (Roche *et al.* 1989). Such an echo is produced when the initial ultraviolet flash and/or flux emitted around the peak of the light curve is absorbed by pre-existing dust near the supernova and re-radiated in the infrared. In addition, Felten & Dwek (1989) have suggested that backscattering of optical radiation will give rise to an optical light echo.

Roche *et al.* (1989) measured an angular diameter for the 10 μm source of 1.5 arcsec. This diameter implies that at least some of the emission must arise as a light echo. If we assume that all of the dust emission is a light echo then the contribution it makes to the data we use to calculate bolometric fluxes must be removed. Some estimate of this contribution can be made using the far-infrared colour temperatures and 10 μm fluxes. Unfortunately this cannot at present be done with any degree of accuracy owing to uncertainty about the properties of the dust.

Table 9 (columns 2 and 3 respectively) contains the 10 μm fluxes and colour temperatures taken from the literature and from various pre-publication sources. The contribution to the 10 μm flux from sources other than dust, largely hydrogen plasma and weak emission lines, was estimated by extrapolating the trend shown by the observations on days 257 and 368 (Aitken *et al.* 1988). The remaining 10 μm flux, which is assumed to originate from dust, is given in

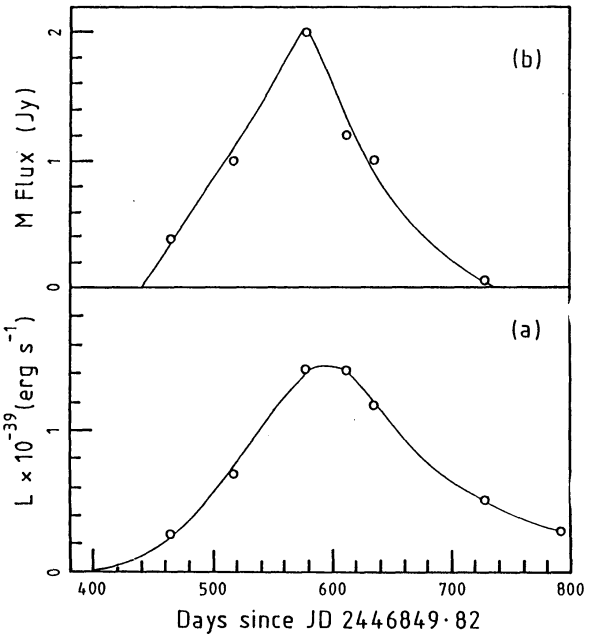

Figure 4. (a) The total energy output from dust as a function of time. (b) The dust contribution to the flux in the *M* band as a function of time. Both figures are based on the data in Table 9.

Table 9. Flux from dust.

Day	F_{10} (Jy)	T_D (K)	F_{10}(dust) (Jy)	F_M(dust) (Jy)	F_{DUST} (10^{-39} erg s^{-1})	Ref
465	4.3	400	2.1	0.38	0.26	1
517	7.0	400	5.6	1.0	0.70	1
578	12.2	400	11.4	2.0	1.42	1
612	12.	350	11.4	1.2	1.41	2
635	10.	350	9.5	1.0	1.17	3
728	3.2	250	3.0	0.05	0.51	4
792	1.1	206	1.1	0.01	0.29	5

References: 1 Roche *et al.* (1989; 2 Witteborn *et al.* (private communication); 3 Moseley *et al.* (1989); 4 Roche *et al.* (private communication); 4 Aitken *et al.* (private communication).

column 4 of Table 9. The dust contribution to the *M* (4.8 μm) flux deduced from this 10 μm flux and the colour temperature is given in column 5. The total energy output from the dust is given in column 6 assuming that it emits like a blackbody at the given colour temperature. Fig. 4 shows a plot of the total energy from the dust and its 4.8 μm flux as a function of time as derived from the data in Table 9. The curves shown are those used in the following discussion.

Fig. 5 shows the relative contribution made to the bolometric magnitude by the *M* flux as measured (open circles) and with the dust component removed (crosses). Thus it would appear that the peak between days 600 and 650 was due to the dust excess in the *M* band. If the dust emission is a light echo then the *M* fluxes should be corrected for its effect before the bolometric magnitude is estimated. Table 10 contains *M* and bolometric magnitudes with this correction applied. With the possible exception of dust, the main contributor to the high flux in the *M* band is CO emission (see Papers III, IV and V). It is rather surprising that the proportion

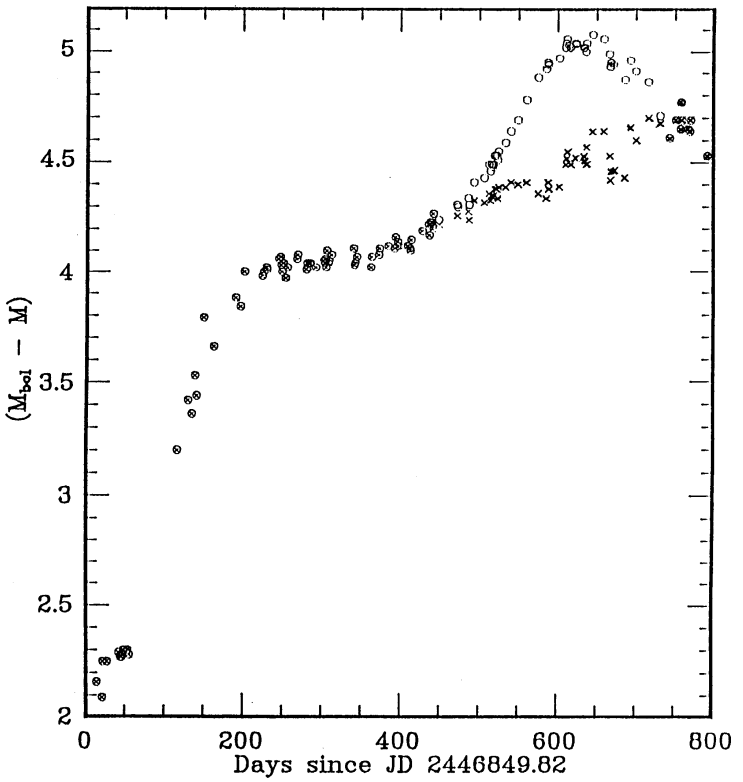

Figure 5. $(M_{bol} - M)$ as a function of time. The values before and after the removal of the contribution from dust are shown as open circles and crosses, respectively.

of the total U to M flux provided by the M band has continued to increase, even after correction for dust effects. It is possible that we are in fact underestimating the effects of dust on the M flux after day 400, but it should be possible to establish this one way or the other if 5 μm spectra are obtained after day 700.

6.2 DUST IN EJECTA

An alternative explanation for the far-infrared emission is that it arises from dust condensed within the ejecta, in which case the flux from the dust must be added to the U to M flux to calculate the total energy output from the supernova. The condensation of dust in the ejecta has been suggested by Danziger *et al.* (1989) as an explanation for observed line asymmetries in the optical spectrum. Spectra observed at the SAAO indicate that the asymmetry in the [O I] line developed between days 560 and 590 (Menzies, in preparation). There is no indication of reddening during the period in which the dust must have formed. Thus if this is the correct explanation the dust may have condensed in clumps mixed with emitting material, in effect producing almost neutral extinction. The colour changes (Section 5) are difficult to explain in this scenario without resorting to extremely peculiar geometry.

7 Total energy output

In Papers III, IV and V we showed that between days 135 and 500 the behaviour of the U to M bolometric light curve together with the hard X-ray and γ-ray flux was consistent with the decay of 0.078 $M_\odot$ ^{56}Co as the sole significant energy source during that period.

Table 10. Bolometric and M magnitudes after subtraction of dust emission.

Day	Mbol	M
486.86	7.31	3.03
487.83	7.35	3.11
493.83	7.41	3.08
506.82	7.60	3.28
512.83	7.69	3.33
514.81	7.72	3.39
515.81	7.73	3.38
516.82	7.75	3.40
517.81	7.77	3.43
518.80	7.78	3.43
519.82	7.78	3.40
520.82	7.81	3.43
522.80	7.84	3.46
523.82	7.86	3.52
524.82	7.86	3.47
533.81	8.02	3.63
540.72	8.14	3.73
549.74	8.30	3.90
560.75	8.51	4.10
575.68	8.80	4.44
585.75	9.01	4.67
587.76	9.04	4.63
588.70	9.06	4.68
602.65	9.31	4.92
610.55	9.47	4.98
611.56	9.48	4.96
612.60	9.48	4.93
614.56	9.52	5.02
616.57	9.57	5.08
623.74	9.70	5.18
633.59	9.82	5.29
634.61	9.84	5.33
636.67	9.88	5.38
637.55	9.86	5.29
645.54	10.02	5.38
659.59	10.23	5.59
666.55	10.37	5.84
667.58	10.40	5.98
668.55	10.43	5.97
671.56	10.45	5.99
686.58	10.69	6.26
693.58	10.71	6.05
700.68	10.86	6.26
716.56	10.98	6.28
731.46	11.23	6.55

In the following discussion we examine the more recent energy output of the supernova and compare it with expectations from radioactive decay. For this purpose, in addition to that of ^{56}Co, the decay of ^{57}Co is included. It is assumed that the solar abundance ratio for isotopes of mass 56 to mass 57 is applicable, in which case ^{57}Co provides 4 per cent of the total radioactive decay energy on day 800 (Woosley, Pinto & Hartmann 1989) and less at earlier times (see Section 9.3).

As discussed above (Section 6) it is not clear whether the far-infrared flux should be included in the calculated total energy output or not. Therefore, in the first instance we exclude

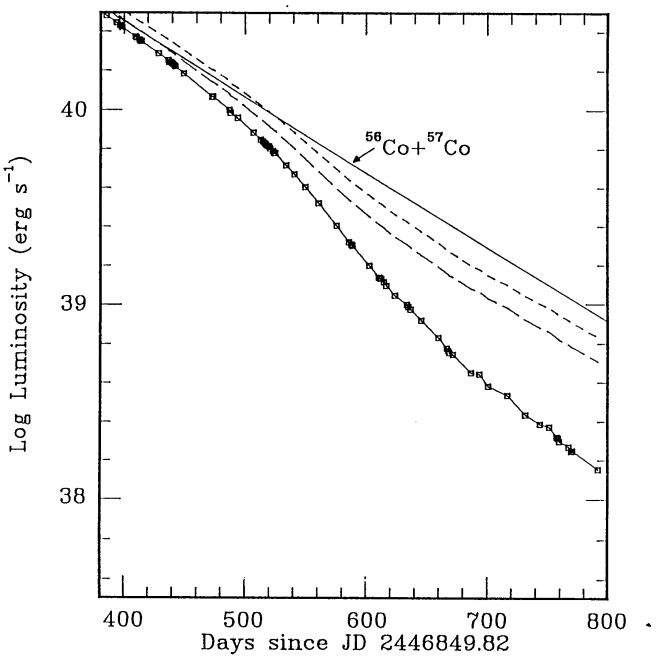

Figure 6. The supernova light curve as a function of time. The points represent the measured *U* to *M* luminosity after making a small correction for the effects of dust emission on *M*. The line of short dashes represents the summation of the predictions of the high energy flux from model 10HMM with the *U* to *M* fluxes. The line of long dashes is a similar summation using model 14E1. Note that after day 550 both of these summations fall short of the solid line which represents the total radioactive decay energy.

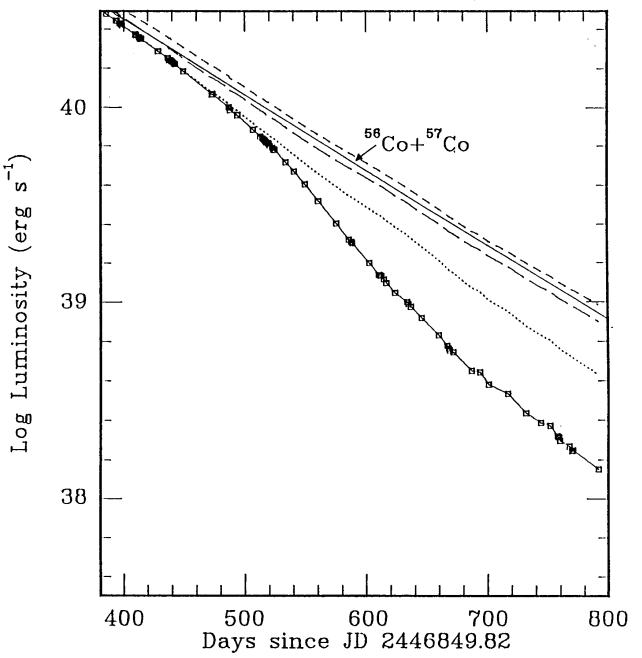

Figure 7. The supernova light curve as a function of time. The points represent the measured *U* to *M* flux after making a small correction for the effects of dust emission on *M*. The dotted line represents the addition of the energy from dust emission, as specified by Fig. 4, to the *U* to *M* observations. The dashed lines represent the addition to the dotted line of the contribution from high-energy luminosity as specified by model 10HMM (short dashes) and model 14E1 (long dashes). The solid line represents the total radioactive decay energy.

it and simply add the U to M bolometric luminosity (with the dust component removed, Table 10) to the X-ray and γ-ray contribution. Ideally we would like to use measured high-energy fluxes for this sum. Such measurements are, however, not available over the full time and frequency range of interest. We must therefore resort to using theoretically modelled fluxes for the high energy range. For this purpose the results from model 10HMM by Woosley *et al.* (1989) and from model 14E1 by Nomoto [private communication, which has similar X-ray and γ-ray fluxes to 11E1 by Kumagai *et al.* (1989) are used]. Both of these models provide reasonable fit to the published X-ray and γ-ray measurements. The result is shown in Fig. 6. It is clear from this figure that the measured energy output from the supernova falls below that expected from radioactive decay. Although there are various ways of achieving a luminosity excess (e.g. energy input from a pulsar, other sources of radioactive decay or a light echo), an apparent deficit is only possible if the energy escapes anisotropically. Therefore, assuming in the first instance that anisotropy is not the explanation, there would appear to be good reasons to add at least some fraction of the far-infrared luminosity into the total energy integral.

The effect of adding the dust luminosity from Fig. 4 to the U to M flux and X-rays and γ-rays is illustrated in Fig. 7. Within the errors there is remarkably good agreement between the total observed energy output of the supernova and the predictions from radioactive decay. This result strongly implies that most of the far-infrared flux originates within the ejecta.

Fig. 8 shows the contribution to the total energy output from the various components. Note the very steep drop in the U to M luminosity at a time when the far-infrared dust output was rising. This also supports the view that dust, formed within the ejecta, is responsible for redistributing some fraction of the optical output into the far-infrared.

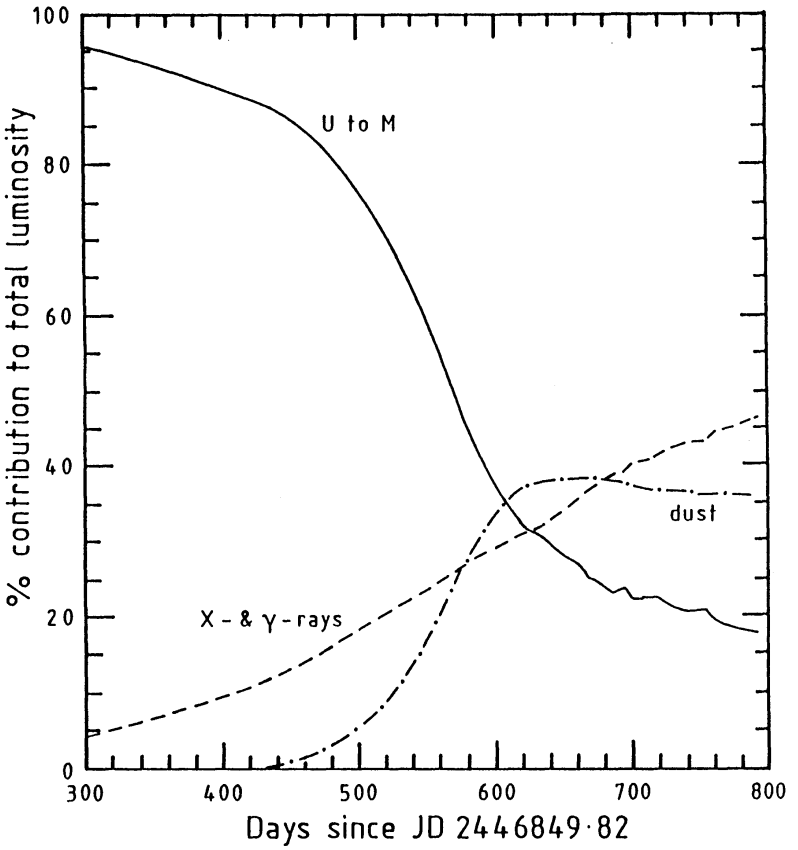

Figure 8. The changing contribution to the total energy balance of the various wavelength ranges, based on Fig. 7.

8 Combined emission from light echo and newly formed dust

It would appear from Section 7 and Fig. 7 that most of the infrared flux must originate in the ejecta. However, the dust energy output as calculated above assumes emission from dust at a particular temperature. If we allow for a range of temperatures, then the total far-infrared energy output will be larger. This taken together with the high uncertainty associated with the X-ray and γ-ray contributions allows for some fraction of the far-infrared to originate from a light echo, as indeed the spatially extended nature of the 10 μm emission indicates it does.

9 Discussion

Although the *U* to *M* observations are becoming increasingly difficult to make, it is still practical to achieve greater frequency and accuracy than is possible for the other important wavelength ranges. It is therefore of some interest to observe the various factors which might affect the shape of the *U* to *M* bolometric light curve either in the period under discussion or in the near future. These factors include the effects of clumping, the emergence of a pulsar and additional sources of radioactive decay, as well as dust formation and light echoes which have already been considered.

9.1 CLUMPING

To explain the shapes of the UVOIR (UltraViolet, Optical and InfraRed) and X-ray light curves it is necessary to assume that mixing of the originally layered supernova ejecta has occurred. It is now generally accepted that Rayleigh–Taylor instabilities during the early expansion phase would have given rise to mixing. It is likely that clumping also occurred, and there is some evidence for this. Kumagai *et al.* (1989) have suggested that the X-ray flux at recent times could only be maintained at the observed relatively high level if clumping had occurred. Models without clumping predict a marked decline in flux that is not observed. High-resolution spectra of the [O I] $\lambda\lambda$6300, 6364 lines made in 1987 December by Stathakis & Cannon (1988) show velocity structure on a scale of 200 km s^{-1} which can plausibly be ascribed to clumping of material in the region where the lines are formed. Finally, the fast moving knots seen in the Cas A supernova remnant seem to indicate that clumping has occurred there.

The *U* to *M* bolometric flux curve can be well reproduced by a simple clumping model that crudely incorporates an angular dependence into the γ-ray deposition function. The angle-averaged deposition of energy into the UVOIR is based upon the predictions of Pinto & Woosley's (1988) Model 10HMM. Simply clumping a medium will not greatly alter the deposition efficiency so long as the optical depth remains large along all angles, but as the average depth falls below unity there will be angles along which γ-rays can escape more freely. We divide the sky, as seen from the centre of the supernova, into regions of solid angle, x and y such that $x+y=1$ and in region x the γ-ray optical depth (or mass column depth) is $f(f>1)$ times the angle averaged value from 10HMM. Region y similarly has optical depth $1/f$ times the average value. The requirement that the angle average of τ remains the same implies $x=1/(f+1)$ and $y=f/(f+1)$, but the overall γ-ray deposition is decreased by this operation since the fraction that escapes, $\exp(-f\tau)/(f+1)+f\exp(-\tau/f)/(f+1)$, is now greater than $\exp(-\tau)$ for $f>1$. We further presume that, once deposited, the γ-radiation is thermalized and emitted isotropically. An example of this effect is given in Fig. 9, which shows the fit to the light curve when $f=1$ until day 500 and then increases linearly with time until $f=5$ by day 640.

This model seems to provide a good fit to the *U* to *M* light curve. Changes in the optical

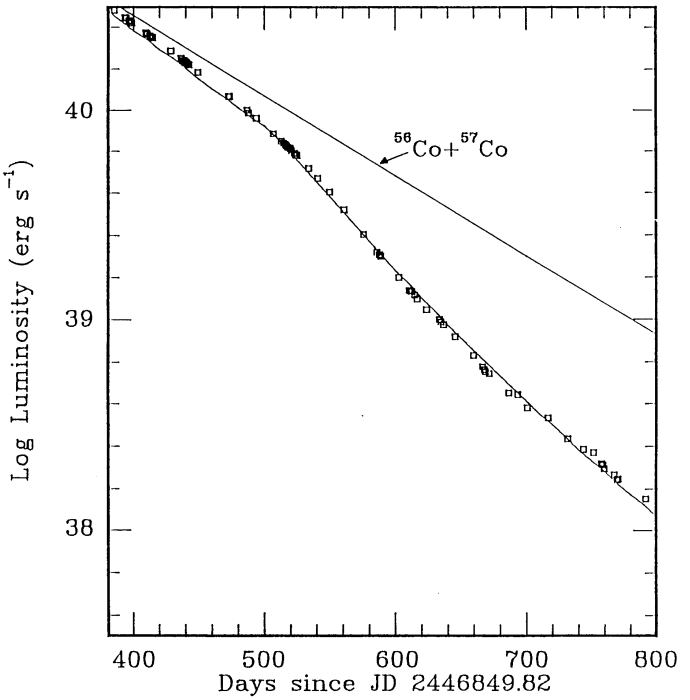

Figure 9. The supernova light curve as a function of time. The points represent the measured *U* to *M* luminosity after making a small correction for the effects of dust emission on *M*. The curve drawn through the points is the predicted UVOIR flux from the clumping model described in Section 9.1. The solid line represents the total radioactive decay energy.

depth with wavelength in the UVOIR range, which might be expected as clumping develops, could provide a more natural explanation of the observed colour changes (see Section 5) than does a dust condensation model.

The evidence from high-energy flux measurements is less clear. Recent γ-ray observations by Barthelmy *et al.* (1989) give fluxes of $6.5 \pm 1.5 \times 10^{-4}$ and $3.1 \pm 0.9 \times 10^{-4}$ photons cm^{-2} s^{-1} for the 847 and 1238 keV lines, respectively, on day 631. These are in good agreement with the predictions of the *unclumped* 10HMM model of 5.38×10^{-4} and 4.36×10^{-4} photons cm^{-1} s^{-1}. The clumpy model discussed above, which gives a good fit to the UVOIR observations, predicts substantially higher fluxes. However, given the errors on the γ-ray and far-infrared contributions to the total energy output, some degree of clumping is still possible, and indeed may be necessary to explain the X-ray fluxes.

9.2 PULSAR

There is general agreement that a pulsar should exist in the centre of SN1987A and it is possible that it has been detected (Middleditch *et al.* 1989). Given the reasonable agreement between the measured total energy and the predictions for radioactive decay there is no pressing need to postulate the presence of additional energy sources in the supernova at this time. However, within the errors involved in the various measurements, it is equally not possible to rule out the existence of a source contributing $< 10^{38}$ erg s^{-1}.

One explanation of the decreased *U* to *M* bolometric decline rate since day 600 (see Table 8) is that energy from the central neutron star is adding directly to the ^{56}Co radioactive decay energy. If this is so then it is possible to make a rough estimate of the additional energy. Subtracting a flux of 8×10^{37} erg s^{-1} from the bolometric luminosity results in an e-folding

time of 60.3 ± 0.3 d from day 500 to 770, i.e. it 'straightens-out' the luminosity curve making the more recent data follow the same decay rate as that shown between days 500 and 600. This procedure is somewhat arbitrary as it assumes that without the addition of the pulsar the light curve would have decayed at the same rate between days 600 and 792 as it did between days 500 and 600. There is no strong justification for this assumption.

If there is an additional energy of around 8×10^{37} erg s^{-1} present then its effects will rapidly dominate those of ^{56}Co decay and this should be obvious very shortly. It will not necessarily be trivial to distinguish between the effects of a pulsar and those of an additional source of radioactive decay (see below and Pinto, Woosley & Ensman 1988).

9.3 ADDITIONAL SOURCES OF RADIOACTIVE DECAY

Additional energy contributions to the total luminosity might arise from other sources of radioactive decay. Isotopes other than ^{56}Co have been considered by Pinto *et al.* (1988) and Kumagai *et al.* (1989). These authors agree that in the period under consideration only ^{57}Co will produce a significant additional contribution. ^{57}Co is produced by the decay of ^{57}Ni and although it is only expected to be present in small quantities (the ratio of isotopes of mass 57 to mass 56 is expected to be between one and two times the solar value of 0.024 for ^{57}Fe/^{56}Fe, Cameron 1982), its long half-life, 271 d compared to 77 d of ^{56}Co, makes it a relatively important contributor at late times. In addition the γ-rays from the decay of ^{57}Co are of a lower energy than those from ^{56}Co and are therefore more easily deposited as UVOIR radiation.

As explained in Section 7, a solar abundance ratio is assumed for calculating the total radioactive decay energy indicated in the figures. Woosley, Pinto & Hartmann (1989) use solar abundance in their model 10HMM, while Kumagai *et al.* (1989) assume twice solar in their model 14E1. Using twice solar abundance will increase the ^{57}Co contribution to the total flux from 4 to 8 per cent, and to the UVOIR from about 7 to 13 per cent, on day 800.

10 Conclusions

The energy output of the supernova between days 135 and 792 can be explained as originating entirely from the decay of radioactive cobalt. A small additional contribution from an infrared light echo was possibly present after day 500. However, a significant fraction of the far-infrared flux probably originated from dust within the ejecta and therefore should be added with the rest of the UVOIR to the X-ray and γ-ray flux to make up the radioactive decay energy. A similar suggestion has been made by Moseley *et al.* (1989). Alternatively it might be possible to explain the form of the UVOIR light curve in terms of clumping of the ejecta. If this explanation is correct then the X-ray and γ-ray fluxes must make up the energy deficit.

There is no definite evidence of additional energy sources during this period, although the errors in the total flux are such that additional sources weaker than 10^{38} erg s^{-1} could be present.

Acknowledgments

We thank Dave Kilkenny for some observations and for supervising the reductions of the optical photometry. We are grateful to Ken Nomoto, Pat Roche, Dave Aitken, Bob Kirshner and F. C. Witteborn for communicating data in advance of publication. We also thank Pat Roche and Ken Nomoto for helpful discussion and Peter Meikle and Jason Spyromilio for help with the AAT observations. We are very grateful to Dave Aitken for pointing out an error in the original manuscript of this paper.

References

Aitken, D. K., Smith, C. H., James, S. D., Roche, P. F., Hyland, A. R. & McGregor, P. J., 1988. *Mon. Not. R. astr. Soc.,* **235,** 19P.

Barthelmy, S., Gehrels, N., MacCallum, C. J., Teegarden, B. J. & Tueller, J., 1989. *IAU Circ. No. 4764.*

Cameron, A. G. W., 1982. In: *Essays in Nuclear Astrophysics*, p. 23, eds Barnes, C. A., Clayton, D. D. & Schramm, D. N., Cambridge University Press, Cambridge.

Catchpole, R. M. *et al.*, 1987. *Mon. Not. R. astr. Soc.,* **229,** 15P. Paper II.

Catchpole, R. M. *et al.*, 1988. *Mon. Not. R. astr. Soc.,* **231,** 75P. Paper III.

Catchpole, R. M. *et al.*, 1989. *Mon. Not. R. astr. Soc.,* **237,** 55P. Paper V.

Danziger, I. J., Gouiffes, C., Bouchet, P. & Lucy, L. B., 1989. *IAU Circ. No. 4746.*

Felten, J. E. & Dwek, E., 1989. *Nature*, **339,** 123.

Fransson, C., Cassatella, A., Gilmozzi, R., Kirshner, R. P., Panagia, N., Sonneborn, G. & Wamsteker, W., 1989. *Astrophys. J.,* **336,** 429.

Gilmozzi, R., 1987. In: *ESO Workshop on the SN1987A Proceedings*, p. 19, ed. Danziger, I. J., ESO, Garching bei München.

Kirshner, R. P., 1987. In: *ESO Workshop on the SN1987A Proceedings*, p. 121, ed. Danziger, I. J., ESO, Garching bei München.

Kumagai, S., Shigeyama, T., Nomoto, K., Itoh, M., Nishimura, J. & Tsurata, S., 1989. *Astrophys. J.,* **345,** in press.

Menzies, J. W. *et al.*, 1987. *Mon. Not. R. astr. Soc.,* **227,** 39P. Paper I.

Middleditch, J. *et al.*, 1989. *IAU Circ. No. 4735.*

Moseley, S. H., Dwek, E., Glaccum, W., Graham, J. R., Loewenstein, R. F. & Silverberg, R. F., 1989. *Nature*, in press.

Pinto, P. A. & Woosley, S. E., 1988. *Nature,* **333,** 534.

Pinto, P., Woosley, S. E. & Ensman, L., 1988. *Astrophys. J.,* **331,** L101.

Roche, P. F., Aitken, D. K., Smith, C. H. & James, S. D., 1989. *Nature,* **337,** 533.

Stathakis, R. & Cannon, R. D., 1988. *AAO Newsletter 45.*

Walborn, N. R., Lasker, B. M., Laidler, V. G. & Chu, Y.-H., 1987. *Astrophys. J.,* **321,** L41.

West, R. M., 1987. In: *ESO Workshop on the SN1987A Proceedings*, p. 5, ed. Danziger, I. J. ESO, Garching bei München.

Whitelock, P. A. *et al.*, 1988. *Mon. Not. R. astr. Soc.,* **234,** 5P. Paper IV.

Woosley, S. E., Pinto, P. A. & Hartmann, D., 1989. *Astrophys. J.,* in press.